PAPER

Unraveling the catalytic mechanisms of H₂ production with thiosemicarbazone nickel complexes†

Alexandre Barrozo [iD]* and Maylis Orio [iD]*

Thiosemicarbazone-based complexes have been explored as a new class of redox-active catalysts H₂ production due to their flexibility for extensive optimization. To rationalize the process, we need to understand how these complexes function. In this work, we used DFT calculations to investigate the various mechanisms that could take place for three previously characterized Ni complexes. We found that two possible mechanisms are compatible with previously published experimental data, involving protonation of two adjacent N atoms close to the metal center. The first step likely involves a proton-coupled electron transfer process from a proton source to one of the distal N atoms in the ligand. From here, a second proton can be transferred either to the coordinating N atom situated in between the first protonated atom and the Ni atom, or to the second distal N atom. The former case then has the protons in close distance for H₂ production. However, the latter will require a third protonation event to occur, which would fall in one of the N atoms adjacent to the Ni center, resulting in a similar mechanism. Finally, we show that the H−H bond formation is the rate-limiting step, and suggest additional strategies that can be taken into account to further optimize these complexes.

Introduction

Hydrogen has been regarded as a promising renewable and non-polluting molecular fuel to answer the world energy demand.[1,2] One of the main challenges lies with strategies of cost-effective and green mass production. The scientific community has been advancing toward finding alternatives to platinum-based catalysts, the golden standard for man-made hydrogen production.[3] This has been possible thanks to continuous research on how hydrogenases produce H₂ in nature.[4–6] As a consequence, innumerous molecular electrocatalysts have been developed, attempting to either reproduce the chemical structure of the active sites in these enzymes (biomimetic),[7–12] or their main mechanistic features (bioinspired).[13–16]

In the past few years, molecular complexes based on thiosemicarbazone ligands have drawn significant attention due to their efficiency, low overpotential requirement and the active role played by the ligand in the hydrogen evolution reaction (HER).[17–22] Thiosemicarbazone ligands are highly customizable, offering the possibility to not only fine-tune the catalytic cycle of the complex, but also to better understand the different ways HER can occur. Thus, it is paramount to understand how these catalysts work, which is the main goal of this work.

We have recently studied a set of mononuclear Ni-thiosemicarbazone (**NiL**) complexes.[23] The idea was to investigate the impact of different phenyl substituents as a strategy of ligand optimization for HER. We have shown that the more electron-withdrawing the substituent was, the less negative the overpotential requirement became. However, simply changing the overpotential was not the best strategy to optimize the complex, as we saw an impact in the turnover rates of H₂ production.

In this article, we considered three catalysts from our previous studies: two of the best catalysts (**NiOCH₃** and **NiSCH₃**), and the best in terms of overpotential, but worst in turnover (**NiCN**). We assessed all the possible mechanisms for HER using DFT, finding two types of pathways that accurately account for multiple experimental observations, such as cyclic voltammograms and UV-Vis spectra, in the presence of trifluoric acid (TFA) acting as the proton source. We show that the catalytic cycle is best described by a [EC][EC] and a [EC][EC]C mechanism occurring concomitantly (Fig. 1), where E describes an electrochemical event, C, a chemical (proton transfer) event, and [EC], a concerted proton-coupled electron transfer (PCET). We show that the latter, involving three protons, is the rate-limiting step, and reproduces trend in kinetics for the three catalysts. Additionally, our data shows that PCET is essential, as it stabilizes the reduction steps by ~0.25 V for different complexes for the first step. We conclude by proposing possible synthetic strategies to design new Ni-thiosemicarbazone catalysts.

Aix-Marseille Univ, CNRS, Centrale Marseille, iSm2, Marseille, France. E-mail: alexandre.hernandes-barrozo@univ-amu.fr; maylis.orio@univ-amu.fr
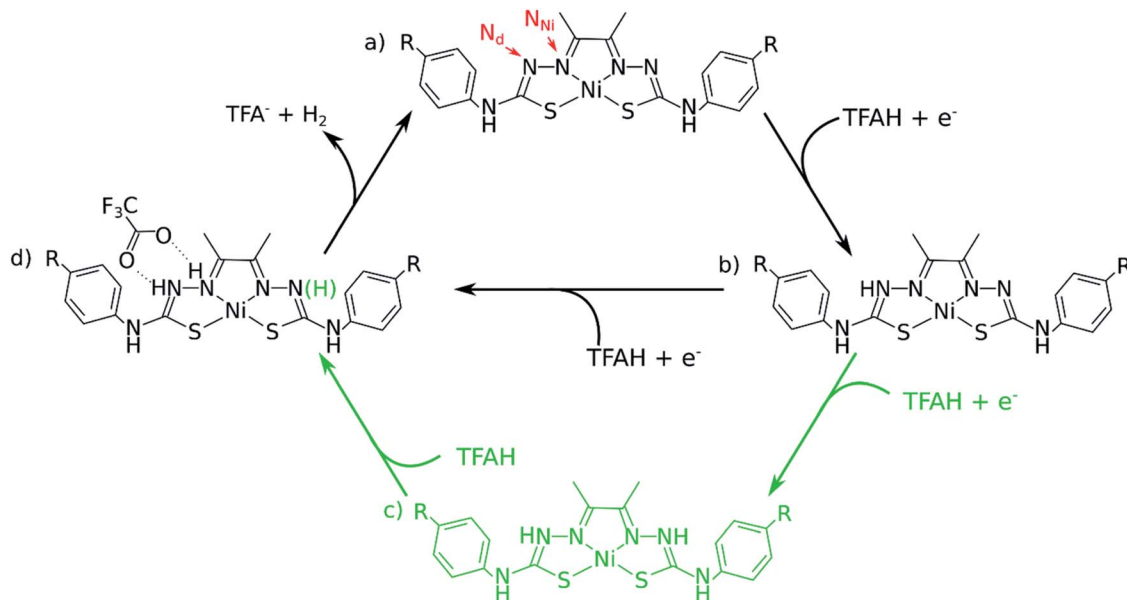
Fig. 1 The two-proton, two-electron proposed catalytic cycle for the series of NiL complexes investigated in this study. R = OCH₃, SCH₃ and CN. In red, we indicate the notation adopted for this article, where N_{Ni} corresponds to the coordinating N atoms, and N_d is the distal N atom further away from Ni. TFA⁻ and TFAH corresponds to the anionic conjugated base and the neutral protonated form of TFA, respectively. Protonation sites were determined based on calculated relative pK_a values. The catalytic cycle begins with the complex in a neutral singlet state (a). The arrival of TFAH will trigger a PCET involving one of the N_d sites, provided that enough potential is applied to the system (b). The process would repeat itself, this time with protonation of an adjacent N_{Ni} atom (d). A possibility of a three-proton scenario is also considered (in green), with both N_d protonated prior to protonation of one of the N_{Ni} atoms (c).

Results and discussion

The first steps: EE, EC, CE, CC or [EC]?

Throughout the article, TFAH refers to protonated neutral form of the acid, while TFA⁻ stands for the anionic conjugated base form. We start by revisiting previous experimental observations on these complexes (Table 1). In cyclic voltammetry experiments in the presence of TFAH, we noticed a single peak at ∼−1.3 V (vs. Fc⁺/⁰), corresponding to the potential necessary to allow for the catalytic cycle to take place.[21,23] Redox potential calculations of those complexes yield a first potential at ∼−1.5 V, and a second at ∼−2.0 V, regardless of the substituent.[19] Unless the presence of TFAH H-bonding the complex would stabilize the second reduction by ∼0.7 V, we could discard a mechanism starting with EE. UV-Vis experiments[21,23] showed that the spectrum does not change in the absence and presence of TFAH. Since it is a strong acid, this finding points to the fact that the complex does not get protonated spontaneously. Thus, we can expect that mechanisms starting with

a chemical step (CE and CC) are not likely to occur. Thus, we would ultimately consider the first steps as being either a stepwise EC process, or a single, concerted, [EC] step. With that in mind, we need to probe how and where the first protonation step occurs.

One of the complications in studying these complexes lies with its multiple protonation sites (Fig. 1). We can disregard the

Table 1 The two reduction potentials for the three **NiL** complexes in the absence of TFA, and the catalytic overpotential in the presence of TFA.[21,23] Potentials (V) refer to Fc⁺/⁰

Complex	$E^0(Ni^{II}L/Ni^{II}L^-)$	$E^0(Ni^{II}L^-/Ni^IL^{2-})$	$E_{cat/2}$ (TFA)
NiOCH₃	−1.57	−2.20	−1.32
NiSCH₃	−1.50	−2.13	−1.33
NiCN	−1.40	−1.99	−1.27

Table 2 Relative values of pK_a for the **NiOCH₃** complex. Values are relative to free energy of protonating either one or both N_d atoms, for the 1st and 2nd protonation events, respectively. The 1st protonation event occurs only in a reduced state

Protonation sites	NiLH⁺	NiLH⁰
1st protonation		
N_d	—	0
N_{Ni}	—	−4.2
S	—	−8.2
Ni	—	−10.8
2nd protonation: without TFAH		
$N_{d,1}$, $N_{d,2}$	0	0
$N_{d,1}$, $N_{Ni,1}$	−6.5	−0.4
$N_{d,1}$, $N_{Ni,2}$	−10.0	−0.6
$N_{d,1}$, S_1	−7.2	−4.1
$N_{d,1}$, S_2	−8.7	−4.6
$N_{d,1}$, Ni	−15.5	−4.3
2nd protonation: with TFAH		
$N_{d,1}$, $N_{d,2}$	0	0
$N_{d,1}$, $N_{Ni,1}$	−2.7	3.1

case where the N atoms from the phenylthiocarbamide fragments are protonated, since adding a second H atom to them yields a very high energy species.[21,24] Due to symmetry, there are four sites to consider: Ni, S, N_{Ni} and N_d. We calculated the relative values of pK_a after the first reduction by comparing free energy differences for each protonation event. We observed that N_d is the most favorable site for the first protonation (Table 2). With this in mind, we proceeded with investigating the energetics of the first proton transfer. This involved assessing the free energies associated with the complex in the presence of a TFAH molecule H-bonding N_d. We analyzed the energies considering the proton either attached to TFA$^-$ (reactant state, RS), or transferred to the complex (product state, PS), also taking into account different oxidation states (*i.e.* **NiL^0**, **NiL$^-$** and **NiL^{2-}**).

Fig. 2 shows a scheme with free energies for every process. On the top, we display the two reduction potentials for each complex in the absence of the proton source. When considering TFAH interacting with the protonation site, a spontaneous proton transfer occurs upon reduction. Furthermore, we notice that the reduction process of the complex is at least 0.2 eV less negative than in the absence of acid (*e.g.* −1.31 *vs.* −1.54 V for **NiOCH$_3$**). This stabilization effect suggests a PCET phenomenon. Such change in reduction potentials was also seen in cyclic voltammograms, in similar magnitude (Table 1).

The following steps: EC, CE or [EC]?

Our calculations show that the first part of the cycle is a PCET to N_d. This means that now we have our complex protonated at one of the N_d atoms, and the protonated complex remain neutral. In principle, what we would need to do at this stage is to simply repeat the previous calculations, now considering a new protonation state of the complex. We start by considering the pK_as of the possible proton acceptors. However, protonation of one site broke the symmetry of the complex, so we need to take into account both sides.

At this stage, we should also consider two different oxidation states: **NiLH$^+$** and **NiLH^0**, corresponding to the second protonation event before and after the second reduction, respectively. Comparison of energetics show that the second reduction state is best described by a singlet state. Table 2 shows the relative

values of pK_a against protonating both N_d sites. We see that most favorable protonation state involves both N_d sites, regardless of the oxidation state. However, due to the structures of the complexes and TFAH, there is a possibility of a double H-bonding interaction for one particular site: the $N_{d,1},N_{Ni,1}$, where two adjacent N atoms would become protonated (Fig. 1 and 3), and this could increase its pK_a. In fact, recalculating the pK_a difference between protonating the adjacent N_{Ni} and the opposite side N_d reduces the pK_a gap to −2.7 units to the adjacent site prior to reduction (**NiLH$_2^+$**), and becomes advantageous by 3.1 units upon reduction (**NiLH$_2^0$**). This double H-bonding advantage is solely present for the N_{Ni} adjacent to the protonated N_d, creating a more stabilizing site for TFAH to bind to the complex, which could favor this kind of interaction between the acid and the complex. Additionally, since the complexes differ in substituents far from the thiosemicarbazone structure, and their electronic structures are very similar (Fig. S1–S3†), relative pK_as will not differ significantly.

We start by assessing the simpler two-proton, two-electron scenario. We performed the same analysis as done above (Fig. 3). Just like with geometry optimization upon reduction of the complex and in the presence of TFAH, the proton transferred is triggered spontaneously. The same kind of stabilizing effect on the redox potentials is observed.

Our results point out to a second PCET, being more advantageous than a stepwise EC process, which features calculated potentials above the measured catalytic potentials (*e.g.* −1.84 *vs.* −1.32 V for **NiOCH$_3$**). Additionally, the calculated PCET redox potentials are below the catalytic potential (*e.g.* −1.02 *vs.* −1.32 V for **NiOCH$_3$**), which makes such process able to take place.

This is not the only possibility: unlike the first part of the cycle, we need to consider a possible proton transfer prior to reduction. Our calculations show that a proton transfer before reduction is energetically favourable for **NiOCH$_3$** and **NiSCH$_3$**, but slightly unfavourable for **NiCN** substituent. Furthermore, the subsequent reduction potentials are also below the catalytic potential, although 40–60 mV more negative than the PCET path (−1.08 *vs.* −1.02 V for **NiOCH$_3$**). As a consequence, we cannot easily discriminate between [EC] and CE at this stage. However, considering that: (i) catalysis would occur at
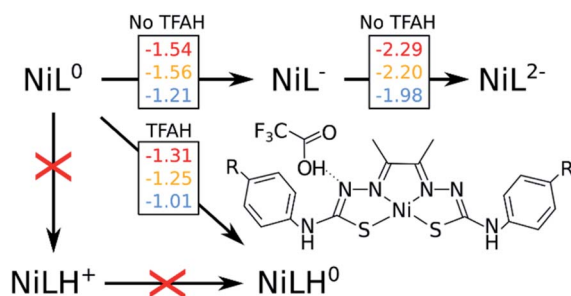

Fig. 2 Free energy diagram considering the first protonation, as well as first and second reduction steps. Red, yellow and blue numbers are free energy differences corresponding to OCH$_3$, SCH$_3$ and CN substituents, respectively. All number are in eV.
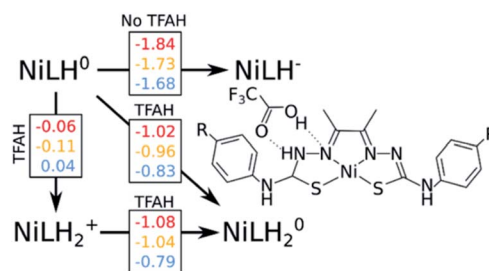

Fig. 3 Free energy diagram considering the second protonation to two adjacent N atoms (N_d and N_{Ni}) and the final step of the cycle. Red, yellow and blue numbers are free energy differences corresponding to OCH$_3$, SCH$_3$ and CN substituents, respectively. All number are in eV.

a potential of ~-1.3 V, (ii) electrons are faster than protons, and (iii) the reduction potential for the PCET event is less negative by about 0.3 V compared to experiment, we could speculate that [EC] is more likely to occur than the stepwise CE. A more detailed study would be required to confirm this hypothesis.

The "three-proton" scenarios

A catalytic cycle for H_2 production does not necessarily need to involve two protons. Hess and co-workers have reported a cobalt complex where three protons are required, with one of them acting as a pre-catalytic preparation of the complex.[25] This possibility could also take place in the kind of catalysts studied here. Table 2 shows that the pK_a for a protonation of the second N_d is favorable prior to a second reduction, regardless of the interactions with TFAH. Thus, we need to take it into account. This would be an intermediate step of a three-proton scenario, where a third proton would eventually bind to N_{Ni}, as expected from Table 2, particularly regarding the interaction between TFAH and the protonated complex. Fig. 4 shows the free energy diagrams of these two steps. While for **NiSCH₃** and **NiCN** we again observe a PCET, for **NiOCH₃** we observe a spontaneous protonation prior to reduction of the complex.

However, reduction of the complex followed by this protonation is now a more expensive process, 50 mV (-1.37 vs. -1.32 V) more negative compared to the first PCET potential. This is important, because depending on the applied potential, we could have only the two-proton mechanism [EC][EC] occurring. For a potential that can attain a -1.32 V reduction, but not a -1.37 V, one could claim that only the two-proton mechanism could occur.

Upon the second protonation, we now need a third proton for H_2 production. Table 2 shows how the pK_as for the N_{Ni} are significantly higher than for S and Ni. Thus, we need to assess how proton transfer would occur at either one of the N_{Ni} atoms. It turns out that, upon placing TFAH in double H-bonding interaction with the complex, proton transfer occurs spontaneously for all complexes when performing geometry optimization, without the need of a third reduction. From here, we should ask if we need a third electron. In principle, the two adjacent protons are in close distance for the reaction to take
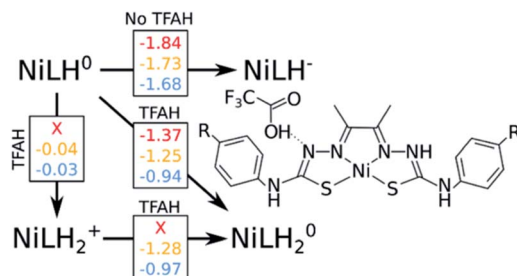
place. However, at the moment that two electrons are transferred to the protons for H_2 formation, the complex will be left as **NiLH⁺**, meaning with one proton and charge +1. On the other hand, if a third reduction occurs, we will restore the first intermediate state of the complex in the catalytic cycle, i.e. after the first PCET. It turns out that the redox potentials of these complexes for the third reduction after the third protonation are too negative: -1.87 V, -1.94 V and -1.58 V for **NiOCH₃**, **NiSCH₃** and **NiCN**, respectively. Since the catalytic potentials are all at ~-1.3 V, we can discard the hypothesis of a third reduction.

The last step: H_2 formation and release

In the last two sections, we saw that there are two possible mechanisms. Both have two adjacent N atoms protonated (Fig. 1d), meaning two protons in close proximity for the formation of H_2. The main difference is the extra protonation of the complex, which leads to a difference in charge. Additionally, the TFA⁻ is still bound by two H-bonds. The results shown above suggest both mechanisms can occur concomitantly. We performed a potential energy surface (PES) scan for the two protons at different distances (see Methodology section and Tables S1–S6†), starting from a larger distance from that of
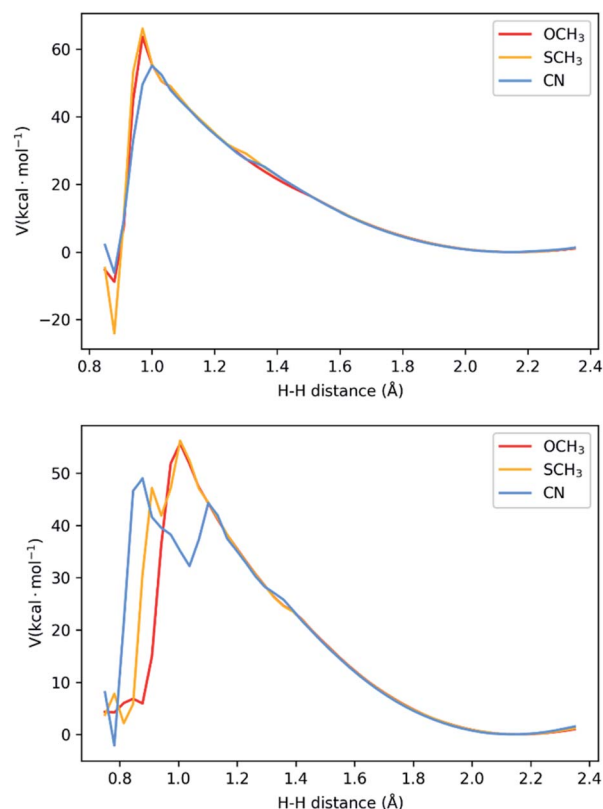

Fig. 5 Potential energy surface for H−H distances for the two-proton, two-electron (top) and three-proton, two electron (bottom) mechanisms. The three-proton mechanism shows the presence of high-energy intermediates for two of the complexes, associated with one proton between TFA⁻ and the bound second proton. See Fig. S4−S6† for representations of the highest energy states.

Fig. 4 Free energy diagram considering the second protonation to the second N_d atom. Red, yellow and blue numbers are free energy differences corresponding to OCH₃, SCH₃ and CN substituents, respectively. The NiOCH₃ complex it spontaneously protonated in the presence of TFAH. All number are in eV.

Table 3 Comparison of calculated activation barriers ($\Delta E^{\ddagger}$), ZPVE, frequencies of vibration of protons in the direction of H_2 formation ($\nu(H_2)$), H_2 turnover rates ($k(H_2)$), and experimental turn over frequencies (TOF$_{max}$)[17,19] for the three NiL complexes

Complex	$\Delta E^{\ddagger}$ (kcal mol^{-1})	ZPVE (kcal mol^{-1})	$\nu(H_2)$ (cm^{-1})	$k(H_2)$ (s^{-1})	TOF$_{max}$ (s^{-1})[17,19]
Two-proton, two-electron mechanism					
NiOCH$_3$	63.8	4.23	2356.4	183.2	89.7
NiSCH$_3$	66.5	4.19	2388.7	110.1	115.9
NiCN	55.1	3.48	2368.4	115.9	10.2
Three-proton, two-electron mechanism					
NiOCH$_3$	55.8	3.30	2341.2	10.8	89.7
NiSCH$_3$	55.5	4.94	2351.5	22.0	115.9
NiCN	49.2	3.65	2445.1	2.8	10.2

equilibrium in the complex (2.35 Å) to the bond length of H_2 (0.75 Å). During the scan, we allowed the remaining atoms to relax and the resulting surface is displayed in Fig. 5. Between 2.35 Å and 1.20 Å, no noticeable change is seen in the interaction between the two protons, the complex and TFA$^-$. As the distance gets shorter, the distance between TFA$^-$ and the complex starts increasing, as the proton bound at N_d detaches from the complex and starts binding to its adjacent proton. This is where we start seeing differences between the complexes. In both mechanisms, NiCN tends to dissociate at a larger distance. Particularly for the three-proton case, the dissociated proton stays at very close distances between TFA$^-$ and the bound proton ($\sim$1.10 Å for both). This could be the reason for the resulting high energy intermediate observed in Fig. 5. As for the other two complexes, the proton behaviour remains similar. Between the highest energy point, at $\sim$1.00 Å, and the product state, there is an abrupt drop in energy. This is due to the fact that H_2 is close to formation, and it dissociates from the complex, together with TFA$^-$. Realistically, this surface would be smoother, as formation of H_2 and its dissociation from the complex would occur concomitantly. Nevertheless, the approach applied here is a computationally affordable method that, as we shall show below, suffices to describe the main differences between the complexes in kinetics for the formation of H_2. Our results show activation barriers in the range of 55–66 kcal mol^{-1} for all complexes. These are very high barriers that would yield slow reaction rates. Nevertheless, such barriers are similarly seen in other intramolecular proton transfer processes.[26–28] In those cases, tunnelling is paramount, and could be assessed from the PES using the semi-classical WKB approximation. Details of this approach can be found in the Methodology section and ref. 28.

We calculated the zero-point vibrational energy (ZPVE) differences associated with the ground and the highest energy states from harmonic analysis. This will give the energy at which the protons will attempt to tunnel through the barrier.[28] We also obtained the frequencies of vibration for the two protons, associated with the mode that would bring them together by fitting a parabola to the PES for H–H distances near equilibrium (1.9–2.35 Å). Those frequencies will tell us with which frequency tunnelling will be attempted. Finally, the probability of tunnelling is calculated from the WKB approximation, and the

kinetic rates are obtained as a product between this probability and the calculated frequency of vibration between the two protons.

Results are summarized in Table 3. We clearly see that the two-proton, two-electron mechanism is the fastest one. Thus, the real limiting step would be the H_2 production for the three-proton, two-electron mechanism. In this case, we see the qualitative agreement between the calculated rates, and kinetic experiments. The underestimation of rates is expected from the WKB approximation.[28] Still, we capture the difference of about one order of magnitude between NiSCH$_3$ and NiCN. Our results show that there is no correlation between activation barriers and the catalytic rates. Rather, it seems to be an interplay between all the parameters involved and the shape of the barrier.

While NiCN possesses a much lower barrier, it has a broader barrier, particularly due to a high-energy intermediate state, involving a proton in between TFA and the second bound proton prior to product release (Fig. 5 and S4–S6†). A similar intermediate is also observed for NiSCH$_3$, but after the highest energy state, and associated only with a very narrow interval of H–H distance. Due to the nature of tunnelling being exponential with the distance,[28] this results in a clear distinction between the reaction rates.

Conclusions

The objective of this work was to figure out how catalysis takes place in three related thiosemicarbazone Ni complexes. We analyzed which catalytic mechanisms would be compatible with experimental observations. Our results show two possible mechanisms, one involving two protons and two electrons, and other with three protons and two electrons. The reactivity occurs at two adjacent N atoms close to the metal center for both pathways, and can happen interchangeably. We saw the importance of including TFA in our calculations to accurately account for the experimentally observed catalytic overpotentials. Our results show that such overpotential corresponds to the first reduction of the complex with a coordinating acid to one of the N_d. The reduction potential is stabilized thanks to a PCET process. From there, the second protonation could occur in two sites: the N_{Ni} adjacent to the first protonated

site, or the second unprotonated N_d. If the second protonated site is the N_{Ni}, the mechanism of H_2 formation would occur *via* tunneling of the two protons. Else, a third proton would have to come into play, being transferred to either N_{Ni}. From there, we would also observe tunneling, albeit one order of magnitude slower than for the former case. Since there is nothing preventing both mechanisms to be happening together, we can claim that the rate-limiting step in the catalytic cycle of these catalysts is the tunneling of the protons on the three-proton pathway. Still, our catalysts would be working with two mechanisms at the same time.

One might argue that studying these complexes with a different acid, even those with a similar structure, such as acetate, could give us the information we need to distinguish between the two pathways. At the same time, nothing prevents the mechanism from changing for different proton sources. In the end, the second half of the cycle has a smaller potential requirement than the first one. This means that any attempt of improving the overpotential requirements of the complex could initially focus in the first half of the cycle. As for the catalytic turnover rate, we essentially want to reduce tunnelling distances without touching the thiosemicarbazone structure. For instance, modifying the complex to increase its ZPVE would be a way to go. This has to go with tandem with no broadening of the activation barrier, which occurred with **NiCN**. These are subjects worth exploring not only for these complexes, but for any intramolecular proton transfer reaction.

Methodology section

DFT calculations

The choice of methodology was based on our previous study.[23] All calculations were performed with ORCA 4.1.2.[29,30] We used BP86, with def2-TZVP as the basis set.[27–34] We used 'Grid4' and 'TightSCF' as our integration and convergence criteria, respectively, following ORCA notation. Solvation effects for DMF were included *via* CPCM.[35] Free energy differences were extracted from numerical frequencies calculations. Since experimental values are reported with respect to the ferrocene electrode in DMF, we need to shift our calculated absolute potentials. We calculated the Gibbs free energy difference for the ferrocene reduction in DMF, obtaining $\Delta G(Fc^{0/+}) = 4.87$ eV. Different oxidation states are described as neutral and singlet for the initial state, doublet after the first reduction, and again singlet after the second reduction. All chemical structure images were generated using Chemcraft.[36]

Tunneling calculations

Tunnelling was considered using the WKB approximation, as shown in ref. 28. The probability of tunnelling is given by

$$T(E) = \exp\left[-2 \int_a^b \frac{2(2m_p)}{\hbar}[V(x) - E]\mathrm{d}x \right]$$

where a and b are the initial and final H–H distances for the protons to tunnel from one well to another of the PES. The intervals of integration were determined based on the

calculated zero-point vibration energy difference between the ground and highest-energy states. Here, we do not say transition state, as the highest-energy state possessed two imaginary frequencies. However, both frequencies are associated with the proton vibrations, as well as with the movement of TFA. V is the potential energy, and E the ground state energy, which includes ZPVE. Lastly, m_p is the mass of the proton, and notice that we are considering twice the mass, since both protons are attempting tunnelling through the barrier at once.

The potential energy surfaces are scanned with 33 points (intervals of 0.05 Å between points). The PES is obtained using a cubic spline, and the integral is solved numerically using the Fortran library QUADPACK, as implemented in the SciPy library.

Conflicts of interest

There are no conflicts to declare.

Acknowledgements

Notes and references

1 J. A. Turner, *Science*, 2004, **305**, 972–974.
2 P. P. Edwards, V. L. Kuznetsov, W. I. F. David and N. P. Brandon, *Energy Policy*, 2008, **36**, 4356–4362.
3 O. T. Holton and J. W. Stevenson, *Platinum Met. Rev.*, 2013, **57**, 259–271.
4 J. C. Fontecilla-Camps, A. Volbeda, C. Cavazza and Y. Nicolet, *Chem. Rev.*, 2007, **107**, 4273–4303.
5 W. Lubitz, H. Ogata, O. Rudiger and E. Reijerse, *Chem. Rev.*, 2014, **114**, 4081–4148.
6 K. A. Vincent, A. Parkin and F. A. Armstrong, *Chem. Rev.*, 2007, **107**, 4366–4413.
7 M. L. Helm, M. P. Stewart, R. Morris Bullock, M. Rakowski DuBois and D. L. DuBois, *Science*, 2011, **333**, 863.
8 M. Y. Darensbourg, E. J. Lyon and J. J. Smee, *Coord. Chem. Rev.*, 2000, **206**, 533–561.
9 T. B. Rauchfuss, *Acc. Chem. Res.*, 2015, **48**, 2107–2116.
10 Z. Li, Y. Ohki and K. Tatsumi, *J. Am. Chem. Soc.*, 2005, **127**, 8950–8951.
11 K. Weber, T. Kramer, H. S. Shafaat, T. Weyhermuller, E. Bill, M. van Gastel, F. Neese and W. Lubitz, *J. Am. Chem. Soc.*, 2011, **141**, 472–481.
12 D. Brazzolotto, M. Gennari, N. Queyriaux, T. R. Simmons, J. Pocault, S. Demeshko, F. Meyer, M. Orio, V. Artero and C. Duboc, *Nat. Chem.*, 2016, **8**, 1054–1060.
13 H. I. Karunadasa, C. J. Chang and J. R. Long, *Nature*, 2010, **464**, 1329–1333.
14 M. Ravazet, V. Artero and M. Fontecave, *Inorg. Chem.*, 2005, **44**, 4786–4795.
15 P. Zhang, M. Wang, Y. Yang, T. Yao and L. Sun, *Angew. Chem.*, 2014, **53**, 13803–13807.

16 E. J. Thompson and L. A. Berben, *Angew. Chem.*, 2015, **54**, 11642–11646.

17 X. Jing, P. Wu, X. Liu, L. Yang, C. He and C. Duan, *New J. Chem.*, 2015, **39**, 1051.

18 W. R. McNamara, *et al.*, *Dalton Trans.*, 2015, **44**, 14265.

19 A. Z. Haddad, B. D. Garabato, P. M. Kozlowski, R. M. Buchanan and C. A. Grapperhaus, *J. Am. Chem. Soc.*, 2016, **138**, 7844.

20 A. Z. Haddad, S. P. Cronin, M. S. Mashuta, R. M. Buchanan and C. A. Grapperhaus, *Inorg. Chem.*, 2017, **56**, 11254.

21 T. Straistari, J. Fize, S. Shova, M. Réglier, V. Artero and M. Orio, *ChemCatChem*, 2017, **9**, 2262.

22 T. Straistari, R. Hardré, J. Fize, S. Shova, M. Réglier, V. Artero and M. Orio, *Chem.–Eur. J.*, 2018, **24**, 8779.

23 M. Papadakis, A. Barrozo, T. Straistari, N. Queyriaux, A. Putri, J. Fize, M. Giorgi, M. Réglier, J. Massin, R. Hardré and M. Orio, *Dalton Trans.*, 2020, **49**, 5064–5073.

24 R. Jain, A. A. Mamun, R. M. Buchanan, P. M. Kozlowski and C. A. Grapperhaus, *Inorg. Chem.*, 2018, **57**, 13486–13493.

25 G. C. Tok, A. T. S. Freiberg, H. A. Gasteiger and C. R. Hess, *ChemCatChem*, 2019, **11**, 3973.

26 P. R. Schreiner, H. P. Reisenauer, D. Ley, D. Gerbig, C.-H. Wu and W. D. Allen, *Science*, 2011, **332**, 1300–1303.

27 M. Schäfer, K. Peckelsen, M. Paul, J. Martens, J. Oomens, G. Berden, A. Berkessel and A. J. H. M. Meijer, *J. Am. Chem. Soc.*, 2017, **139**, 5779–5786.

28 H. Quanz and P. R. Schreiner, *J. Comput. Chem.*, 2019, **40**, 543–547.

29 F. Neese, *Wiley Interdiscip. Rev.: Comput. Mol. Sci.*, 2012, **2**, 73–78.

30 F. Neese, *Wiley Interdiscip. Rev.: Comput. Mol. Sci.*, 2018, **8**, e1327.

31 J. P. Perdew, *Phys. Rev. B: Condens. Matter Mater. Phys.*, 1986, **33**, 8822–8824.

32 J. P. Perdew, *Phys. Rev. B: Condens. Matter Mater. Phys.*, 1986, **34**, 7406.

33 A. D. Becke, *Phys. Rev. A: At., Mol., Opt. Phys.*, 1988, **38**, 3098–3100.

34 A. Schaefer, C. Huber and R. Ahlrichs, *J. Chem. Phys.*, 1994, **100**, 5829–5835.

35 V. Barone and M. Cossi, *J. Phys. Chem. A*, 1998, **102**(11), 1995–2001.

36 *Chemcraft – Graphical software for visualization of quantum chemistry computations*, https://www.chemcraftprog.com.

© 2021 The Author(s). Published by the Royal Society of Chemistry